第 32 卷第 8 期
2016 年 8 月

无 机 化 学 学 报
CHINESE JOURNAL OF INORGANIC CHEMISTRY

Vol.32 No.8
1311-1318

# 具有单分子磁行为的二维 Dy(Ⅲ)-配合物

杨玉亭* 屠长征 姚立峰 李俊莉 陈 广 成飞翔
(曲靖师范学院化学化工学院,曲靖 655011)

**摘要**:在水热条件下,利用刚性配体 Hapca(3-氨基吡嗪-2-羧酸)合成了一例基于双核镝结构基元的二维网格配合物$[Dy_2(apca)_4(OH)_2(H_2O)_2]_n$ (**1**)。磁性研究表明:该配合物显示铁磁耦合,并具有典型的慢弛豫行为,其弛豫时间 $\tau_0=9.47\times10^{-7}$ s,各向异性能垒 $U_{eff}/k_B=73.7$ K,是一例少见的具有单分子磁行为的镧系二维网格配合物。

**关键词**:二维;镝;双核;单分子磁体
**中图分类号**:O614.342 **文献标识码**:A **文章编号**:1001-4861(2016)08-1311-08
**DOI**:10.11862/CJIC.2016.185

## Single Molecule Magnet Behavior in a Two-Dimensional Array of Dysprosium(Ⅲ) Complex

YANG Yu-Ting* TU Chang-Zheng YAO Li-Feng LI Jun-Li CHEN Guang CHENG Fei-Xiang
(*College of Chemistry and Chemical Engineering, Qujing Normal University, Qujing, Yunnan* 655011, *China*)

**Abstract:** A two-dimensional (2D) network $[Dy_2(apca)_4(OH)_2(H_2O)_2]_n$ (**1**), which consisted of dinuclear $Dy_2$ units, was gained by utilization of the rigid ligand 3-aminopyrazine-2-carboxylic acid (Hapca) through hydrothermal synthetic approach. Complex **1** displays ferromagnetic coupling and slow magnetic relaxation with $\tau_0=9.47\times10^{-7}$ s and $U_{eff}/k_B=73.7$ K, presenting the rare 2D array of lanthanide single molecule magnet (SMM). CCDC: 1438299.

**Keywords:** two-dimensional; dysprosium; dinuclear; single molecule magnet

## 0 Introduction

Design and synthesis of SMMs continue to attract great attention, not only because of their interests in fundamental physics, but also for their potential application in high-density data storage or devices for future quantum computers[1-3]. An SMM is a discrete molecule that exhibits the super-paramagnet-like property of slow relaxation of the magnetization at low temperature[1a]. Assembling SMMs into coordination polymers of various dimensionalities incorporating either covalent or non-covalent interactions became an appealing new goal for chemists and physicists working in molecular magnetism, because the control of such SMM architectures may provide a unique opportunity to investigate new magnetic behaviors and also the frontier between SMMs and classical bulk magnets[4-8]. To date, only limited 2D and 3D covalently bonded SMMs have been recorded, and most of them are focused on Mn-SMMs[5-6] and Co-SMMs[7]. Following the increasing knowledge about lanthanide SMMs, the design, preparation and magnetic studies of 2D array of lanthanide SMMs seems more interesting. In 2008 and 2009, Murugesu et al. reported two possible 2D array of lanthanide SMMs[8b-8c], however, taking into the large span between SMM centers, we think the so-called quasi 2D array of lanthanide SMMs more suitable for the cases of discrete clusters. Very

收稿日期:2016-02-27。收修改稿日期:2016-06-22。
上海师范大学上海市稀土功能材料重点实验室和云南省科技厅(No.201401CB00299)资助项目。
*通信联系人。E-mail:18288438002@163.com

recently, Yue and co-works reported a dysprosium coordination polymer which features a 2D network structure with dinuclear units and exhibits the frequency dependent peaks[9]. However, the adjacent 2D networks were packed into 3D supermolecular framework by significant hydrogen bond interactions. Thereby, there is still no truly 2D array of lanthanide SMMs.

Herein, we report a two-dimensional Dy-based complex, $[Dy_2(apca)_4(OH)_2(H_2O)_2]_n$ (**1**), where Hapca=3-aminopyrazine-2-carboxylic acid, synthesized by the reaction of Hapca with $Dy_2O_3$ under hydrothermal reaction conditions. Based on the query on the CSD database, we find that the crystal data of **1** has been documented[10], however, the record that we can find is only the crystal data, and the authors only gave the structure description of it. As a potential magnetic material, the previous studies are obviously insufficient. Thus, for **1**, there are still more investigations for us to explore, such as thermostability and magnetic studies. Notably, **1** is stable in the solid state upon extended exposure to air, and has poor solubility in common organic solvents at room temperature, such as alcohol, acetonitrile, DMF, DMA and DMSO.

## 1 Experimental

### 1.1 Materials and measurements

All the chemical regents were purchased commercially and were used as received without further purification. Elemental analyses for C, H, and N were performed on a Perkin-Elmer 240 analyzer. IR spectra were recorded as KBr pellets on a Nicolet Magna-FT-IR 560 spectrometer in the 4 000~400 $cm^{-1}$ regions. The magnetic measurements were performed on the Quantum Design SQUID MPMS XL-7 instruments in a magnetic field of 1000 Oe in the temperature range of 2 ~300 K. The thermogravimetric analyses were investigated on a standard TG analyzer under a nitrogen flow at a heating rate of 5 ℃·$min^{-1}$ for all measurements.

### 1.2 Preparation of complex 1

A mixture of $Dy_2O_3$ (0.373 g, 1.0 mmol), Hapca (0.278 g, 2.0 mmol) in the molar ratio of 1:2 was added into 8 mL of $H_2O/C_2H_5OH$ (5:3, *V*/*V*). Consequently, the resulting solution was transferred and sealed in a 25 mL Teflon-lined stainless steel vessel, which was heated at 170 ℃ for 60 h. After the reactor was slowly cooled to room temperature at a rate of 5 ℃·$h^{-1}$, pure yellow block-shaped crystals were filtrated off, and dried in air. Yield: 66% based on Dy. Elemental analysis Calcd. for $C_{20}H_{22}Dy_2N_{12}O_{12}$(%): C 25.35, H 2.34, N 17.74; Found (%): C 25.71, H 2.17, N 17.21. IR (KBr, $cm^{-1}$): 3 469 (s), 3 402 (vs), 3 270 (s), 1 652(s), 1 602(vs), 1 553 (s), 1 461 (s), 1 407 (s), 1 387 (s), 1 329 (m), 1 233 (m), 1 179 (s), 922 (m), 831 (s), 706 (m), 686 (m), 565 (m), 491 (m).

### 1.3 X-ray crystallography and structure determination

Accurate unit cell parameters of complex **1** were determined by a least-squares fit of $2\theta$ values, and intensity data were measured on a Bruker SMART 1000 CCD diffractometer with Mo $K\alpha$ radiation ($\lambda$ = 0.071 073 nm) at 296 K. The intensity was corrected for Lorentz and polarization effects as well as for empirical absorption based on multi-scan technique. Empirical absorption corrections were applied using the SADABS program[11a] for the Bruker area detector. The structure was solved by direct method and refined by full-matrix least-squares fitting on $F^2$ by SHELX-97[11b-12]. All non-hydrogen atoms were refined anisotropically, the hydrogen atoms of organic ligand were located by geometrically and those of water molecules were determined by different Fourier maps. Crystal data and structure refinement parameters for **1** are summarized in Table 1. Selected bond distances and angles are listed in Table 2.

CCDC: 1438299.

## 2 Results and discussion

### 2.1 Structural description of 1

Complex **1** crystallizes in the monoclinic space group $P2_1/c$. As shown in Fig.1a, the fundamental building unit is a dinuclear Dy(Ⅲ) structure. Both Dy1 and Dy2 sites are eight-coordinated by three oxygen atoms and two nitrogen atoms from three different apca ligands, one oxygen atom from terminal

**Table 1　Crystallographic data for 1**

| | | | |
|---|---|---|---|
| Empirical Formula | $C_{20}H_{22}Dy_2N_{12}O_{12}$ | $D_c$ / (g·cm$^{-3}$) | 2.076 |
| Formula weight | 947.5 | $F$(000) | 1 816 |
| Crystal system | Monoclinic | Crystal size / mm | 0.37×0.32×0.27 |
| Space group | $P2_1/c$ | $\theta$ range / (°) | 1.91~25.00 |
| $a$ / nm | 1.007 0(8) | Limiting indices ($h$, $k$, $l$) | −11~11, −12~13, −24~31 |
| $b$ / nm | 1.174 9(10) | Reflections collected, unique | 12 052, 5 254 |
| $c$ / nm | 2.688 1(19) | Data, restrains, parameters | 5 254, 28, 421 |
| $\beta$ / (°) | 107.58(3) | Goodness-of-fit on $F^2$ | 1.001 |
| $V$ / nm$^3$ | 3.032(4) | Final $R$ indices [$I>2\sigma(I)$] | $R_1$=0.050 8, $wR_2$=0.137 4 |
| $Z$ | 4 | $R$ indices (all data) | $R_1$=0.068 7, $wR_2$=0.147 3 |

**Table 2　Selected bond lengths (nm) and bond angles (°) for complex 1**

| | | | | | |
|---|---|---|---|---|---|
| Dy(1)-O(11) | 0.230 3(5) | Dy(1)-N(1) | 0.268 7(6) | Dy(2)-O(6) | 0.245 2(6) |
| Dy(1)-O(10) | 0.237 4(5) | Dy(1)-N(4) | 0.275 8(6) | Dy(2)-O(4) | 0.248 3(5) |
| Dy(1)-O(9) | 0.244 7(6) | Dy(2)-O(11) | 0.238 7(6) | Dy(2)-N(10) | 0.272 2(7) |
| Dy(1)-O(3) | 0.245 8(6) | Dy(2)-O(10) | 0.228 7(5) | Dy(2)-N(7) | 0.272 2(6) |
| Dy(1)-O(5) | 0.245 9(5) | Dy(2)-O(12) | 0.248 6(6) | | |
| Dy(1)-O(2) | 0.247 0(5) | Dy(2)-O(7) | 0.246 2(5) | | |
| | | | | | |
| O(11)-Dy(1)-O(10) | 70.06(18) | O(5)-Dy(1)-N(1) | 135.77(19) | O(10)-Dy(2)-O(12) | 79.52(19) |
| O(11)-Dy(1)-O(9) | 79.94(19) | O(2)-Dy(1)-N(1) | 63.82(18) | O(11)-Dy(2)-O(12) | 123.91(19) |
| O(10)-Dy(1)-O(9) | 125.87(18) | O(11)-Dy(1)-N(4) | 80.40(18) | O(6)-Dy(2)-O(12) | 76.8(2) |
| O(11)-Dy(1)-O(3) | 138.65(18) | O(10)-Dy(1)-N(4) | 135.69(19) | O(7)-Dy(2)-O(12) | 118.16(19) |
| O(10)-Dy(1)-O(3) | 150.37(18) | O(9)-Dy(1)-N(4) | 77.9(2) | O(4)-Dy(2)-O(12) | 148.77(18) |
| O(9)-Dy(1)-O(3) | 75.9(2) | O(3)-Dy(1)-N(4) | 62.10(18) | O(10)-Dy(2)-N(10) | 104.62(18) |
| O(11)-Dy(1)-O(5) | 100.22(19) | O(5)-Dy(1)-N(4) | 72.1(2) | O(11)-Dy(2)-N(10) | 71.9(2) |
| O(10)-Dy(1)-O(5) | 81.26(18) | N(1)-Dy(1)-N(4) | 148.7(2) | O(6)-Dy(2)-N(10) | 101.1(2) |
| O(9)-Dy(1)-O(5) | 149.56(18) | Dy(1)-O(11)-Dy(2) | 109.4(2) | O(7)-Dy(2)-N(10) | 63.82(18) |
| O(3)-Dy(1)-O(5) | 85.1(2) | O(10)-Dy(2)-O(11) | 70.10(18) | O(4)-Dy(2)-N(10) | 136.8(2) |
| O(11)-Dy(1)-O(2) | 150.00(18) | O(10)-Dy(2)-O(6) | 137.25(17) | O(12)-Dy(2)-N(10) | 71.8(2) |
| O(10)-Dy(1)-O(2) | 80.09(18) | O(11)-Dy(2)-O(6) | 151.62(18) | O(10)-Dy(2)-N(7) | 78.39(18) |
| O(9)-Dy(1)-O(2) | 117.16(19) | O(10)-Dy(2)-O(7) | 150.42(19) | O(11)-Dy(2)-N(7) | 135.29(18) |
| O(3)-Dy(1)-O(2) | 71.32(18) | O(11)-Dy(2)-O(7) | 80.34(18) | O(6)-Dy(2)-N(7) | 62.30(18) |
| O(5)-Dy(1)-O(2) | 77.48(18) | O(6)-Dy(2)-O(7) | 72.16(19) | O(7)-Dy(2)-N(7) | 126.30(18) |
| O(11)-Dy(1)-N(1) | 102.87(18) | O(10)-Dy(2)-O(4) | 99.37(19) | O(4)-Dy(2)-N(7) | 70.94(19) |
| O(10)-Dy(1)-N(1) | 72.1(2) | O(11)-Dy(2)-O(4) | 83.56(18) | O(12)-Dy(2)-N(7) | 78.4(2) |
| O(9)-Dy(1)-N(1) | 72.2(2) | O(6)-Dy(2)-O(4) | 83.85(19) | Dy(2)-O(10)-Dy(1) | 110.4(2) |
| O(3)-Dy(1)-N(1) | 101.0(2) | O(7)-Dy(2)-O(4) | 77.63(18) | | |

coordinated water molecule and two oxygen atoms from the $\mu_2$-OH$^-$ groups. The polyhedron with donor atoms around the Dy1 is shown in Fig.1b, and Muetterties′ approach can be used here to analyze the coordinate geometry of Dy(Ⅲ) ion[13]. The data of $\delta$ and $\varphi$ indicates the coordination polyhedron around the Dy(Ⅲ) ion can be attributed to a distorted trigonal dodecahedron.

Notably, this dinuclear Dy(Ⅲ) unit is highly rare as it is only bridged by two $\mu_2$-OH$^-$ bridges. The Dy-O-Dy angles and Dy⋯Dy distance is *ca.* 110° and ca. 0.38 nm, respectively. Further, through the carboxyl oxygen atoms of apca anions these identical dinuclear fragments are combined together, generating a two-

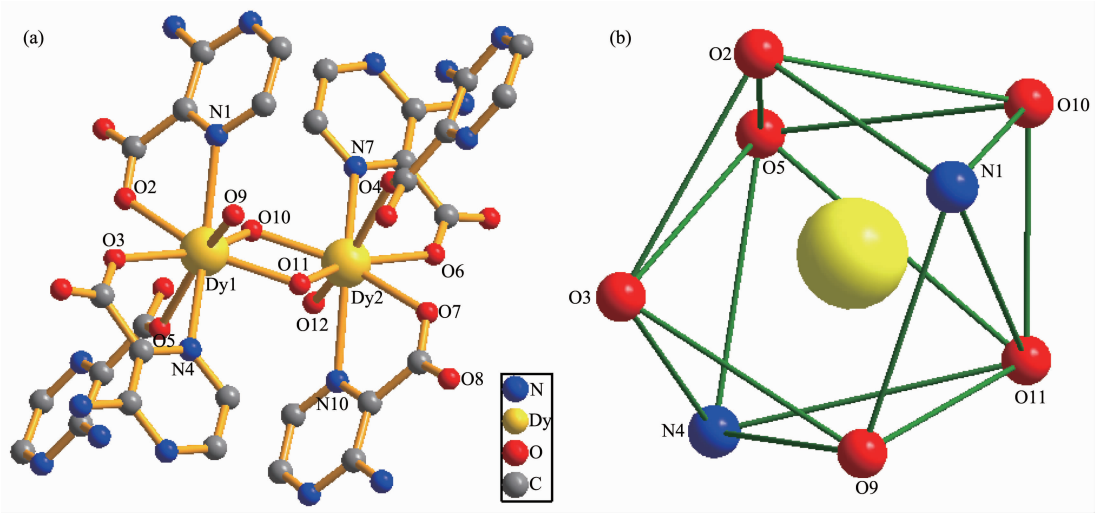


Hydrogen atoms are omitted for clarity

Fig.1 (a) Perspective view of the local coordination environment in **1**; (b) Distorted trigonal dodecahedra coordination of the Dy1

dimensional network (Fig.2). By contrast to the two reported quasi 2D array of lanthanide SMMs, the neighboring $Dy_2$ units in this 2D net are bridged by one apca carboxyl group with the span of ca. 0.6 nm, which means that from the viewpoint of structure the present one is possibly a truly 2D array of lanthanide SMM.

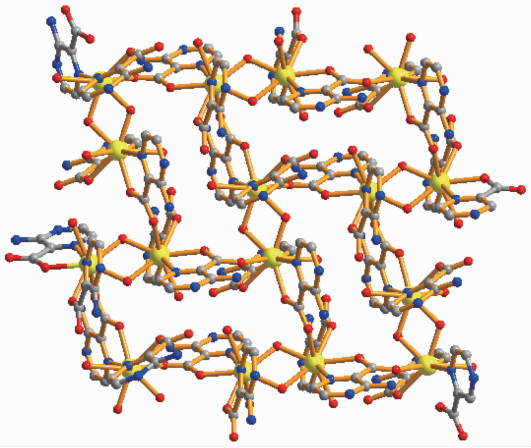

Fig.2 View of 2D network of complex **1**

## 2.2 Thermogravimetric analysis and PXRD

To examine the thermal stability of complex **1**, thermogravimetric analyses (TGA) was carried out in the temperature range of 30~900 ℃ (Fig.3a). From the first plateau we can conclude that complex **1** can be stable up to 280 ℃. Upon further heating, the structure begins to collapse, following the ligand molecules being released. The remaining residue is presumed to be $Dy_2O_3$ (Calcd. 39.37%; Found 38.61%). One strong exothermic peak at 321 ℃ can be observed in the DSC curve, which corresponds to the breakdown of the framework, being in good agreement with the TGA results.

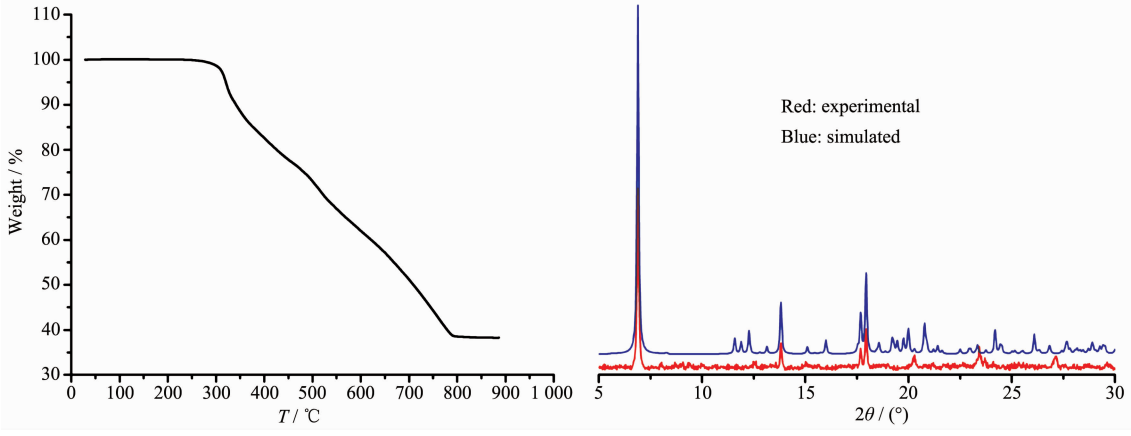


Fig.3 (a) TGA curve of complex **1**; (b) Experimental and simulated PXRD patterns of **1**

The powder X-ray diffraction (PXRD) analysis has also been carried out for complex **1**. The measured PXRD pattern of 1 is in good agreement with the pattern simulated from the respective single-crystal data, confirming the bulk purity of the samples (Fig.3b).

### 2.3 Magnetic property

Temperature-dependent magnetic susceptibility for **1** was measured in an applied magnetic field of 1 000 Oe in the temperature range of 2~300 K (Fig. 4). The $\chi_M T$ value at 300 K is 27.99 $cm^3 \cdot K \cdot mol^{-1}$, which is in good agreement with the expected value of 28.34 $cm^3 \cdot K \cdot mol^{-1}$ for two noninteracting Dy(Ⅲ) ions (Dy(Ⅲ): $S$=5/2, $L$=5, $^6H_{15/2}$, $g$=4/3; $C$=14.17 $cm^3 \cdot K \cdot mol^{-1}$) [14]. Upon cooling, the $\chi_M T$ curve decreases slowly, reaching a minimum of 26.44 $cm^3 \cdot K \cdot mol^{-1}$ at about 28 K, which is mainly ascribed to the progressive depopulation of excited Stark sublevels. Then increases sharply to a maximum value of 41.64 $cm^3 \cdot K \cdot mol^{-1}$ at 2 K, which obviously suggests the presence of intramolecular strong ferromagnetic interactions between Dy(Ⅲ) spin carries as observed in other dinuclear systems[8c].

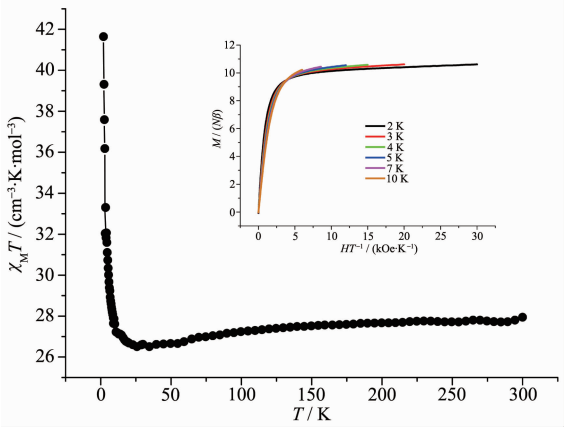


Inset: $M$ vs $H/T$ plot between 2 and 10 K

Fig.4 Temperature dependence of $\chi_M T$ at 1 000 Oe for complex **1**

The best Curie-Weiss law ftting of $\chi_M^{-1}$ vs $T$ from 300 to 2 K gives the Curie constant $C$=27.75 $cm^3 \cdot K \cdot mol^{-1}$ and the Weiss constant $\theta$=−0.53 K. The negative Weiss constant as well as the decrease of $\chi_M T$ value with decreasing temperature may presumably be ascribed to the crystal field effect, the large magnetic anisotropy and the progressive thermal depopulation of the excited Stark sublevels of the Dy(Ⅲ) ions.

The $M$ vs $H/T$ (Fig.4, inset) data at different temperatures below 10 K show a rapid increase of the magnetization at low magnetic fields, which eventually reaches the value of 10.47$N\beta$ at 2 K under 60 kOe without clear saturation. This is expected for materials having ferromagnetically coupled spins. The lack of a clear saturation on the $M$ vs $H/T$ data further confirms the effects arising from low-lying excited states and/or anisotropy. The value is lower than the expected saturation value of 20$N\beta$ (10$N\beta$ for each Dy(Ⅲ) ions) likely due to anisotropy and important crystal-field effects[14b] at the Dy(Ⅲ) ion that eliminates the 16-fold degeneracy of the $^6H_{15/2}$ ground state[15]. Indeed, The maximum of magnetization is in good agreement with the expected value (2×5.23$N\beta$) for two isolated Dy(Ⅲ) ions with a value of 5.23$N\beta$ per Dy(Ⅲ) ion assuming the presence of considerable ligand-field effects[16]. The high-field variation and the non-superposition on a single master curve of the $M$ vs $H/T$ data suggest the presence of a significant magnetic anisotropy and/or low-lying excited states in these systems. Moreover, the material of **1** has no clear hysteresis effect at 2 K with sweep rates used in a traditional SQUID magnetometer (Fig.5).

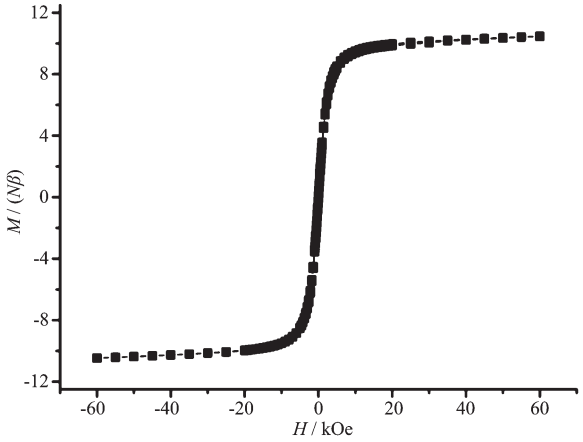


Fig.5 $M$ vs $H$ data of complex **1** at 2.0 K showing the absence of hysteresis effect

The frequency and temperature dependencies of the alternating current (ac) susceptibility measurements were carried out for complex **1** under zero-dc field to investigate the dynamics of the magnetization

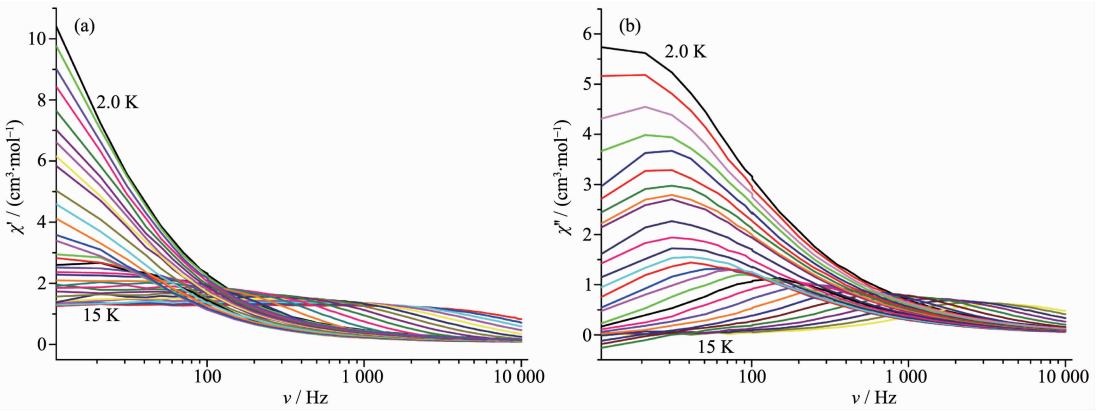


Fig.6 Frequency dependence of the in-phase ($\chi'$, a) and out-of-phase ($\chi''$, b) ac susceptibility from 2.0 to 3.4 K at an interval of 0.2 K and from 3.5 to 15 K at an interval of 0.5 K under zero-dc field for **1**

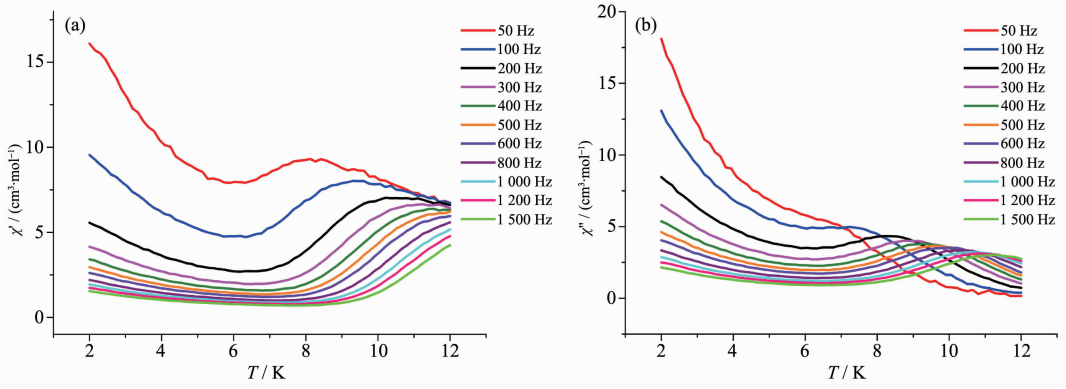


Fig.7 Temperature dependence under zero-dc field of the in-phase ($\chi'$, a) and the out-of-phase ($\chi''$, b) ac susceptibility component at different ac frequency for **1**

(Fig.6 and 7), which show the strong frequency and temperature dependences. Both of them reveal the presence of slow relaxation of the magnetization, which are the typical features associated with SMM behavior.

The relaxation time at different temperatures was extracted by fitting the $\chi''_{ac}$ vs frequency curves[17] (Fig. 7b). The magnetization relaxation rate ($1/\tau$) follows the Arrhenius equation. Plotting the relaxation time versus the reciprocal temperature afforded the Arrhenius plot (Fig.8). This is the characteristic behavior for a thermally activated Orbach process. The theoretical equation for this process is given as:

$$\frac{1}{\tau}=\frac{1}{\tau_0}\exp\left(-\frac{U_{\text{eff}}}{k_{\text{B}}T}\right) \qquad (\mathbf{1})$$

Where $U_{\text{eff}}$ is the effective anistropy energy barrier, $k_{\text{B}}$ is the Boltzmann constant, and $T$ is the temperature. The red line in Fig.8a shows the result of a least-squares fit of the ac susceptibility relaxation data to Eq.(**1**). The best fitting results gave the relaxation time $\tau_0=9.47\times10^{-7}$ s and the energy barrier $U_{\text{eff}}/k_{\text{B}}=73.7$ K. This value of energy barrier is relative higher than some other reported values for polynuclear SMMs[8b,18], exceeds that observed in the two reported quasi 2D array of lanthanon SMMs, and the relaxation time is consistent with the expected value covering $10^{-6}$~$10^{-11}$ s for a typical SMM[19].

From frequency dependences of the ac susceptibilities measurements, Cole-Cole plots (Fig. 8b) in the form of $\chi''$ vs $\chi'$ with nearly semi-circle shape have also been obtained. These data have been fitted to the generalized Debye model[20], giving the small distribution coefficient $\alpha$ value of 0.02~0.14 ($\alpha$= 0 for a Debye model between 6.0 and 13.5 K), indicating the narrow distribution of relaxation times at these temperatures. All these magnetic features support the SMM nature of this remarkable 2D complex.

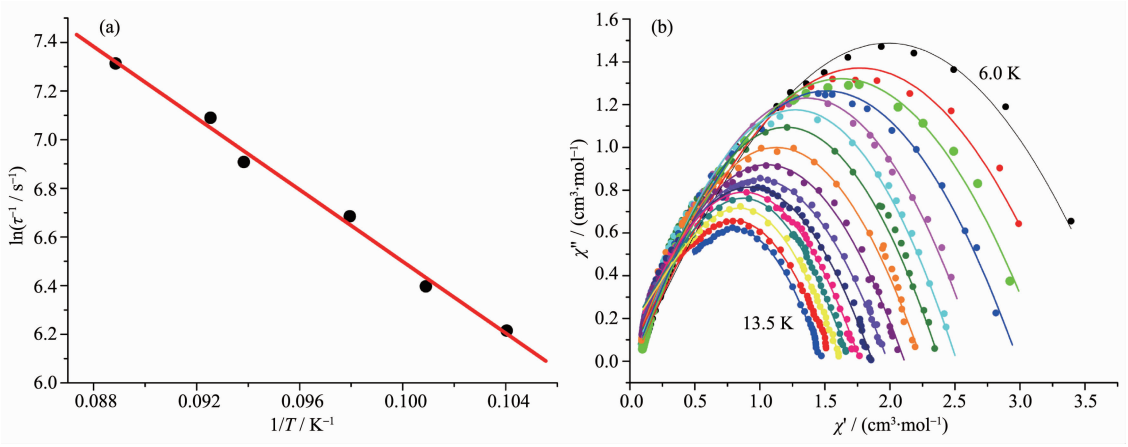


Solid lines are the best fits to the experimental data

Fig.8　(a) Plot of natural logarithm of rate ($1/\tau$) vs inverse of temperature ($1/T$) for complex **1** in the temperature range of 7.5~11.2 K; (b) Cole-Cole plots measured from 6.0 to 13.5 K at an interval of 0.5 K and zero-dc field

## 3　Conclusions

In conclusion, based on 3-aminopyrazine-2-carboxylic acid, a 2D complex which consisted of dinuclear Dy (Ⅲ) units has been prepared and structurally and magnetically characterized. Ac susceptibility measurements reveal frequency-dependent signals, indicative of slow relaxation of magnetization and a relatively large energy barrier (73.7 K). It is confirmed that using highly anisotropic lanthanide building blocks is an effective approach for creating novel SMMs. And more detailed studies are currently carried out to probe further the properties of magnetization in lanthanide clusters with different topologies.

## References:


[1] (a)Sessoli R, Gatteschi D, Caneschi A, et al. *Nature*, **1993**, **365**:141-143

(b)Woodruff D N, Winpenny R E P, Layfield R A. *Chem. Rev.*, **2013**,**113**:5110-5148

[2] (a)Gavey E L, Hareri M A, Reqier J, et al. *J. Mater. Chem. C*, **2015**,**3**:7738-7747

(b)Song Y M, Luo F, Luo M B, et al. *Chem. Commun.*, **2012**, **48**:1006-1008

(c)Chen L, Wang J, Wei J M, et al. *J. Am. Chem. Soc.*, **2014**, **136**:12213-12216

(d)Aulakh D, Pyser J B, Zhang X, et al. *J. Am. Chem. Soc.*, **2015**,**137**:9254-9257

[3] (a)Xue S F, Zhao L, Guo Y N, et al. *Chem. Commun.*, **2012**, **48**:8946-8948

(b)Blagg R J, Ungur L, Tuna F, et al. *Nat. Chem.*, **2013**,**5**: 673-678

(c)Zou H H, Wang R, Chen Z L. *Dalton Trans.*, **2014**,**43**: 2581-2587

(d)Gorczyński A, Kubicki M, Pinkowicz D, et al. *Dalton Trans.*, **2014**,**44**:16833-16839

(e)Cao W, Zhang Y H, Wang H L, et al. *RSC Adv.*, **2015**,**5**: 17732-17737

[4] (a)Wernsdorfer W, Aliaga-Alcalde N, Hendrickson D N, et al. *Nature*, **2002**,**416**:406-409

(b)Long J, Habib F, Lin P H, et al. *J. Am. Chem. Soc.*, **2011**, **133**:5319-5328

(c)Ren M, Bao S S, Hoshino N, et al. *Chem. Eur. J.*, **2013**, **19**:9619-9628

[5] Jeon I, Clérac R. *Dalton Trans.*, **2012**,**41**:9569-9586

[6] (a)Roubeau O, Clérac R. *Eur. J. Inorg. Chem.*, **2008**:4325-4342

(b)Miyasaka H, Nakata K, Lecren L, et al. *J. Am. Chem. Soc.*, **2006**,**128**:3770-3783

(c)Miyasaka H, Nakata K, Sugiuara K I, et al. *Angew. Chem. Int. Ed.*, **2004**,**43**:707-711

[7] (a)Galloway K W, Schmidtmann M, Sanchez-Benitez J, et al. *Dalton Trans.*, **2010**,**39**:4727-4729

(b)Burzurí E, Campo J, Falvello L R, et al. *Chem. Eur. J.*, **2011**,**17**:2818-2822

[8] (a)Chen M, Saudo E C, Jiménez E, et al. *Inorg. Chem.*, **2014**, **53**:6708-6714

(b)Savard D, Lin P H, Burchell T J, et al. *Inorg. Chem.*, **2009**,**48**:11748-11754

(c)Lin P H, Burchell T J, Clérac R, et al. *Angew. Chem. Int. Ed.*, **2008**,**47**:8848-8851

(d)Yi X H, Calvez G, Daiguebonne C, et al. *Inorg. Chem.*, **2015**,**54**:52135219

[9] Yue Y M, Yan P F, Sun J W, et al. *Inorg. Chem. Commun.*, **2015**,**54**:5-8

[10]Deng Z P, Kang W, Huo L H, et al. *Dalton Trans.*, **2010**,**39**: 6276-6284

[11](a)Sheldrick G M. *SADABS*, University of Göttingen, Germany, **1996**.

(b)Sheldrick G M. *SHELXL*-97, *Programs for X-ray Crystal Structure Refinement*, University of Göttingen, Göttingen, Germany, **1997**.

[12]Sheldrick G M. *SHELXS*-97, *Programs for X-ray Crystal Structure Solution*, University of Göttingen, Göttingen, Germany, **1997**.

[13](a)Muetterties E L, Guggenberger L J. *J. Am. Chem. Soc.*, **1974**,**96**:1748-1756

(b)Casanova D, Llunell M, Alemany P, et al. *Chem. Eur. J.*, **2005**,**11**:1479-1494

(c)Liu Q Y, Li Y L, Xiong W L, et al. *CrystEngComm*, **2014**,**16**:585-590

[14](a)Xu G F, Wang Q L, Gamez P, et al. *Chem. Commun.*, **2010**,**46**:1506-1508

(b)Ma Y, Xu G F, Yang X, et al. *Chem. Commun.*, **2010**, **46**:8264-8266

[15]Gao Y J, Xu G F, Zhao L, et al. *Inorg. Chem.*, **2009**,**48**: 11495-11497

[16]Zheng Y Z, Lan Y, Anson C E, et al. *Inorg. Chem.*, **2008**, **47**:10813-10815

[17]Poneti G, Bernot K, Bogani L, et al. *Chem. Commun.*, **2007**: 1807-1809

[18]Guo Y N, Xu G F, Gamez P, et al. *J. Am. Chem. Soc.*, **2010**, **132**:8538-8539

[19]Bernot K, Bogani L, Caneschi A, et al. *J. Am. Chem. Soc.*, **2006**,**128**:7947-7956

[20]Aubin S M J, Sun Z, Pardi L, et al. *Inorg. Chem.*, **1999**,**38**: 5329-5340